

日本原子力研究開発機構機関リポジトリ
Japan Atomic Energy Agency Institutional Repository

Title	Electronic structure and magnetism of the diluted magnetic semiconductor Fe-doped ZnO nanoparticles
Author(s)	Kataoka Takashi, Kobayashi Masaki, Sakamoto Yuta, Song G. S., Fujimori Atsushi, Chang F.-H., Lin H.-J., Huang D. J., Chen C. T., Okochi Takuo, Takeda Yukiharu, Okane Tetsuo, Saito Yuji, Yamagami Hiroshi, Tanaka Arata, Mandal S. K., Nath T. K., Karmakar D., Dasgupta I.
Citation	Journal of Applied Physics, 107(3), p.033718_1-033718_7
Text Version	Publisher
URL	http://jolissrch-inter.tokai-sc.jaea.go.jp/search/servlet/search?5024438
DOI	http://dx.doi.org/10.1063/1.3294620
Right	Copyright (2010) American Institute of Physics. This article may be downloaded for personal use only. Any other use requires prior permission of the author and the American Institute of Physics. The following article appeared in (Appl. Phys. Lett. 107, 033718 (2010)) and may be found at (http://dx.doi.org/10.1063/1.3294620).

Electronic structure and magnetism of the diluted magnetic semiconductor Fe-doped ZnO nanoparticles

T. Kataoka, M. Kobayashi, Y. Sakamoto, G. S. Song, A. Fujimori, F.-H. Chang, H.-J. Lin, D. J. Huang, C. T. Chen, T. Ohkochi, Y. Takeda, T. Okane, Y. Saitoh, H. Yamagami, A. Tanaka, S. K. Mandal, T. K. Nath, D. Karmakar, and I. Dasgupta

Citation: *Journal of Applied Physics* **107**, 033718 (2010); doi: 10.1063/1.3294620

View online: <http://dx.doi.org/10.1063/1.3294620>

View Table of Contents: <http://scitation.aip.org/content/aip/journal/jap/107/3?ver=pdfcov>

Published by the [AIP Publishing](#)

Articles you may be interested in

[Evidence of a cluster glass-like behavior in Fe-doped ZnO nanoparticles](#)

J. Appl. Phys. **115**, 17E123 (2014); 10.1063/1.4864246

[X-ray magnetic dichroism in the \(Zn,Co\)O diluted magnetic semiconductors from first principle calculations](#)

J. Appl. Phys. **111**, 073702 (2012); 10.1063/1.3699276

[Photoluminescence studies on structural defects and room temperature ferromagnetism in Ni and Ni-H doped ZnO nanoparticles](#)

J. Appl. Phys. **108**, 023906 (2010); 10.1063/1.3460644

[The role of Zn interstitials in cobalt-doped ZnO diluted magnetic semiconductors](#)

Appl. Phys. Lett. **96**, 211905 (2010); 10.1063/1.3437082

[Reversible ferromagnetic spin ordering governed by hydrogen in Co-doped ZnO semiconductor](#)

Appl. Phys. Lett. **95**, 172514 (2009); 10.1063/1.3257733

The new SR865 *2 MHz Lock-In Amplifier* ... \$7950



SR865 2 MHz DSP Lock-In Amplifier

Features:

- Intuitive front-panel operation
- Touchscreen data display
- Save data & screen shots to USB flash drive
- Embedded web server and iOS app
- Synch multiple SR865s via 10 MHz timebase I/O
- View results on a TV or monitor (HDMI output)

Specs:

- 1 mHz to 2 MHz
- 2.5 nV/√Hz input noise
- 1 μs to 30 ks time constants
- 1.25 MHz data streaming rate
- Sine out with DC offset
- GPIB, RS-232, Ethernet & USB

SRS Stanford Research Systems
www.thinkSRS.com · Tel: (408)744-9040

Electronic structure and magnetism of the diluted magnetic semiconductor Fe-doped ZnO nanoparticles

T. Kataoka,^{1,b)} M. Kobayashi,¹ Y. Sakamoto,¹ G. S. Song,¹ A. Fujimori,^{1,2} F.-H. Chang,³ H.-J. Lin,³ D. J. Huang,³ C. T. Chen,³ T. Ohkochi,² Y. Takeda,² T. Okane,² Y. Saitoh,² H. Yamagami,^{2,4} A. Tanaka,⁵ S. K. Mandal,⁶ T. K. Nath,⁶ D. Karmakar,^{7,a)} and I. Dasgupta⁸

¹Department of Physics and Department of Complexity Science and Engineering, University of Tokyo, Bunkyo-ku, Tokyo 113-0033, Japan

²Synchrotron Radiation Research Center, Japan Atomic Energy Agency, Sayo-gun, Hyogo 679-5148, Japan

³National Synchrotron Radiation Research Center, Hsinchu 30076, Taiwan

⁴Department of Physics, Faculty of Science, Kyoto Sangyo University, Kyoto 603-8555, Japan

⁵Department of Quantum Matter, ADSM, Hiroshima University, Higashi-Hiroshima 739-8530, Japan

⁶Department of Physics and Meteorology, Indian Institute of Technology, Kharagpur 721302, India

⁷Technical Physics and Prototype Engineering Division, Bhabha Atomic Research Center, Mumbai 400085, India

⁸Department of Solid State Physics and Center for Advanced Materials, Indian Association for the Cultivation of Science, Jadavpur Kolkata 700032, India

(Received 27 July 2009; accepted 19 December 2009; published online 9 February 2010)

We have studied the electronic structure of Fe-doped ZnO nanoparticles, which have been reported to show ferromagnetism at room temperature, by x-ray photoemission spectroscopy, resonant photoemission spectroscopy, x-ray absorption spectroscopy, and x-ray magnetic circular dichroism (XMCD). From the experimental and cluster-model calculation results, we find that Fe atoms are predominantly in the Fe³⁺ ionic state with mixture of a small amount of Fe²⁺ and that Fe³⁺ ions are dominant in the surface region of the nanoparticles. It is shown that the room temperature ferromagnetism in the Fe-doped ZnO nanoparticles primarily originated from the antiferromagnetic coupling between unequal amounts of Fe³⁺ ions occupying two sets of nonequivalent positions in the region of the XMCD probing depth of ~ 2 – 3 nm. © 2010 American Institute of Physics. [doi:10.1063/1.3294620]

I. INTRODUCTION

There is a growing interest in diluted magnetic semiconductors (DMSs), where magnetic ions are doped into the semiconductor hosts, due to the possibility of utilizing both charge and spin degrees of freedom in the same materials, allowing us to design a new generation spin electronic devices with enhanced functionalities.^{1,2} Theoretical studies on the basis of Zener's *p-d* exchange model have shown that wide-gap semiconductors such as ZnO doped with transition metal are promising candidates for room temperature ferromagnetic DMSs.³ First-principle calculations by Sato and Katayama–Yoshida⁴ have also predicted that ZnO-based DMSs exhibit ferromagnetism using local-spin-density-approximation (LSDA) calculation. Subsequently, a number of experiments on ZnO-based DMSs in bulk, thin film, and nanoparticle forms revealed ferromagnetic properties,^{5–10} and among them ZnO-based DMSs nanoparticles have attracted much attention.^{11,12} Current interest in such magnetic nanoparticle systems is motivated by unique phenomena such as superparamagnetism,¹³ quantum tunneling of magnetization,¹⁴ and, particularly, magnetism induced by surface effects.¹⁵ In the nanoparticle form, the structural and electronic properties are modified at the surface as a result of

the broken translational symmetry of the lattice or dangling bond formation, giving rise to weakened exchange coupling, site-specific surface anisotropy, and surface spin disorder.^{16,17} That is, the modification of the electronic structure at the surface of the nanoparticles plays a crucial role in the magnetism of this system.

Recently, Karmakar *et al.*¹⁸ have reported room temperature ferromagnetism in Fe-doped ZnO (ZnO:Fe) nanoparticles in the proposed core/shell structure, where Fe²⁺ ions are situated mostly in the core and Fe³⁺ ions in the surface region. However, LSDA+U calculation¹⁹ has indicated the insulating antiferromagnetic state to be more stable than the ferromagnetic state for ZnO:Fe system. Also, there has been a considerable recent work²⁰ suggesting that structurally perfect ZnO-based DMSs do not exhibit ferromagnetic order. These reports^{19,20} imply that not only the magnetic dopants themselves but also the defects are necessary for ferromagnetism. In view of the presence of Fe³⁺ ions, as indicated by local magnetic probes such as electron paramagnetic resonance (EPR) and Mössbauer measurements, Karmakar *et al.*¹⁸ have proposed that the presence of surface Zn vacancies that dope hole into the system will be more effective to stabilize the ferromagnetism in this system. In order to understand the ferromagnetic interaction in this system and to contribute to new material design, experimental investigation of the electronic structure of the ZnO:Fe nanoparticles is important. However, correlation between the magnetic properties

^{b)}Electronic mail: kataoka@wyvern.phys.s.u-tokyo.ac.jp.

^{a)}Present address: Max Planck Institut Fur Festkörperforschung, Heisenbergstrasse 1, Stuttgart D-70569, Germany.

and the electronic structure of the ZnO:Fe nanoparticle semiconductors has not been clarified yet. In this paper, we have investigated the electronic structure of ZnO:Fe nanoparticles using x-ray photoemission spectroscopy (XPS), resonant photoemission spectroscopy (RPES), x-ray absorption spectroscopy (XAS), and x-ray magnetic circular dichroism (XMCD). RPES is a convenient tool to obtain the Fe 3*d* partial density of states (PDOS) in the valence-band spectra.²¹ By performing RPES in the Fe 3*p*-3*d* core-excitation region, we have studied the electronic states in the surface region with a probing depth of ~ 0.5 –1 nm (Ref. 22) of the nanoparticles utilizing the surface sensitivity of the technique. On the other hand, RPES in the Fe 2*p*-3*d* core-excitation region is more bulk sensitive with a probing depth of ~ 1.0 –2 nm (Ref. 22) and enables us to study the electronic structure in both the core and surface regions of the nanoparticles. XAS and XMCD, whose probing depth are ~ 2 –3 nm, enable us to study the element specific electronic structure of the ZnO:Fe nanoparticles. In particular, XMCD is a powerful tool to study element-specific local magnetic states. Based on our experimental results, we shall discuss the origins of the ferromagnetic properties and magnetic interactions in the ZnO:Fe nanoparticles.

II. EXPERIMENTAL

Our samples, ZnO:Fe nanoparticles, were made of nanocrystalline 10%-Fe-doped ZnO powder, which was synthesized by using the chemical pyrophoric reaction method.¹⁸ Structural characterization was carried out using x-ray diffraction (XRD) and transmission electron microscopy (TEM), demonstrating a clear nanocrystal phase. As observed by TEM, the average particle size was around 7 nm with the particle size distribution of 3–30 nm. Magnetization measurements on the same samples revealed a ferromagnetic-to-paramagnetic transition temperature > 450 K. Details of the sample preparation were described in Ref. 18. We measured a pressed pellet sample, which, after grinding, had been calcined at 620 K. The ferromagnetic moment per Fe, as deduced from the superconducting quantum interference device (SQUID) magnetization data, was $\sim 0.05\mu_B$ at room temperature.¹⁸ XAS and XMCD measurements were performed at the Dragon Beamline BL11A of National Synchrotron Radiation Research Center (NSRRC) in the total-electron-yield (TEY) mode (probing depth ~ 2 –3 nm). The monochromator resolution was $E/\Delta E > 10\,000$ and the circular polarization of x-rays was $\sim 55\%$. XPS measurements using the photon energy of $h\nu = 1253.6$ eV were performed at BL23-SU of SPring-8. RPES measurements in the Fe 2*p*-3*d* and 3*p*-3*d* core-excitation regions were performed at BL23-SU of SPring-8 and at BL-18A of Photon Factory (PF), respectively. For the photoemission measurements, all binding energies (E_B) were referenced to the Fermi level (E_F) of the sample holder which was in electrical contact with the sample. The total energy resolutions of the XPS and RPES measurements were ~ 400 and ~ 170 meV, respectively. All the experiments were performed at room temperature.

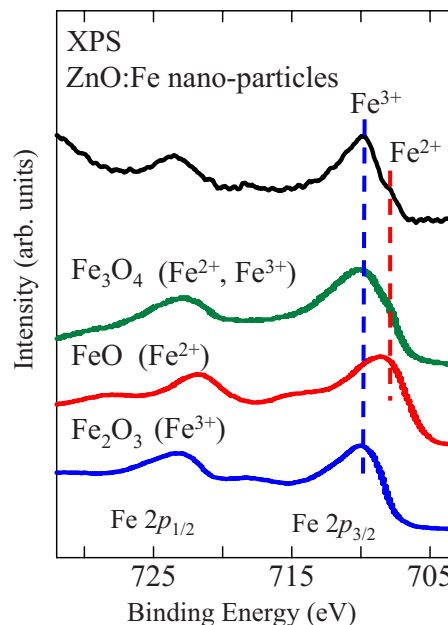


FIG. 1. (Color online) Fe 2*p* core-level XPS spectrum of the ZnO:Fe nanoparticles compared with the XPS spectra of α -Fe₂O₃ (Ref. 23), FeO (Ref. 23), and Fe₃O₄ (Ref. 24).

III. RESULTS AND DISCUSSION

Figure 1 shows the Fe 2*p* core-level XPS spectrum of the ZnO:Fe nanoparticles in comparison with those of α -Fe₂O₃ (Fe³⁺),²³ FeO (Fe²⁺),²³ and Fe₃O₄ (Fe³⁺-Fe²⁺ mixed-valence).²⁴ The Fe 2*p*_{3/2} peak of the ZnO:Fe nanoparticles is split into two peaks at $E_B \sim 710$ and ~ 708 eV, corresponding to the energy positions of α -Fe₂O₃ and FeO. The XPS spectrum of the ZnO:Fe nanoparticles therefore reflects an Fe³⁺-Fe²⁺ mixed-valent state of the Fe ions in agreement with the previous Mössbauer report.¹⁸ In a Fe-doped ZnO system, the valence state of Fe is expected to be 2+ if Fe simply substitutes for Zn. The presence of Fe³⁺ ions in this sample has been suggested to be due to surface Zn vacancies¹⁸ or excess oxygens of the nanoparticles.

In order to study the electronic states in the surface region of the nanoparticles, we performed RPES measurements in the Fe 3*p*-3*d* core-excitation region. RPES in 3*d* transition metals and their compounds are caused by interference between direct photoemission from the 3*d* level and Auger-electron emission following the 3*p*(2*p*)-3*d* core excitation.²¹ Therefore, the difference between valence-band spectra measured on and off resonance is used to extract the resonantly enhanced Fe 3*d* contributions to the valence-band region. Figure 2(a) shows the valence-band photoemission spectra of the ZnO:Fe nanoparticles taken with various photon energies in the Fe 3*p*-3*d* core-excitation region marked on the Fe 3*p*-3*d* XAS spectrum [see Fig. 2(b)]. In the Fe 3*p*-3*d* XAS spectrum, one can see that a peak appears at 58 eV, representing the Fe 3*p*-3*d* absorption. The same peak is found at 58 eV for α -Fe₂O₃ (Fe³⁺).²⁵ For FeO (Fe²⁺), on- and off-resonance energies are reported to be 57 and 53 eV, respectively.²⁶ From this comparison, we conclude that 3*p*-3*d* absorption is mainly due to Fe³⁺ ions. Figure 2(c) shows a magnified view near the valence-band maximum. In

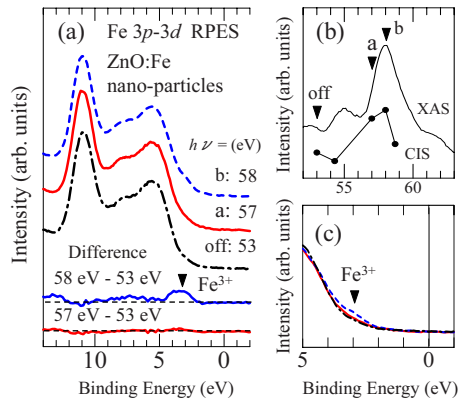


FIG. 2. (Color online) Valence-band photoemission spectra of the ZnO:Fe nanoparticles. (a) A series of photoemission spectra taken with photon energies in the Fe 3*p*-3*d* core-excitation region. Difference curves at the bottom represent the Fe 3*d* PDOS. (b) Fe 3*p*-3*d* XAS and CIS ($E_B \sim 3.4$ eV) spectra. (c) Magnified view near the valence-band maximum.

Fig. 2(c), one can see that in going from the off-resonance spectrum ($h\nu=53$ eV) to 58 eV, the tale at $E_B \sim 3-4$ eV grows in intensity. By subtracting the off-resonance spectrum from the on-resonance ones of Fe^{3+} ($h\nu=58$ eV) and Fe^{2+} ($h\nu=57$ eV), respectively, we have extracted the Fe 3*d* PDOS of Fe^{3+} and Fe^{2+} , as shown in the bottom panel of Fig. 2(a). The Fe^{3+} 3*d* PDOS reveals a feature at $E_B \sim 3-4$ eV. On the other hand, the Fe^{2+} 3*d* PDOS reveals no clear feature. For the Fe 3*p*-3*d* core-excitation region ($h\nu=53-58$ eV), features due to Fe $M_{2,3}M_{4,5}M_{4,5}$ Auger-electron emission are observed around $E_B > 5$ eV,²⁵ indicating that the enhanced features around $E_B \sim 3-4$ eV in our RPES spectra are not due to Auger emission but is due to resonance photoemission. In addition, we note that the line shape of the constant-initial-state (CIS) spectrum at $E_B \sim 3.4$ eV is similar to that of XAS spectrum [see Fig. 2(b)]. We therefore conclude that the Fe^{3+} ions are dominant in the surface region of the ZnO:Fe nanoparticles probed by Fe 3*p*-3*d* RPES. This, together with the bulk-sensitive Fe 2*p*-3*d* RPES result described below, may support the core/shell model of the ZnO:Fe nanoparticles proposed in Ref. 18.

Figure 3(a) shows the Fe 2*p*-3*d* XAS and XMCD spec-

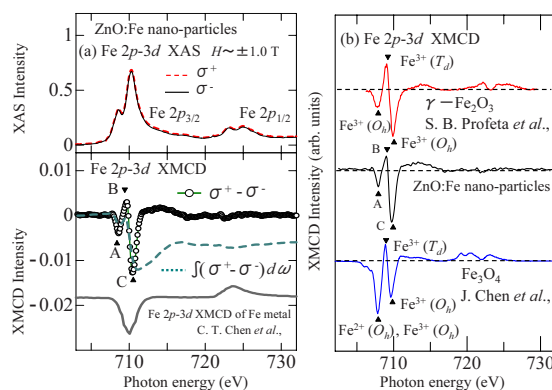


FIG. 3. (Color online) Fe 2*p*-3*d* XAS and XMCD spectra of the ZnO:Fe nanoparticles compared with those of other Fe oxides. (a) Fe 2*p*-3*d* XAS spectra in magnetic fields of ± 1 T. XAS (σ^+ and σ^-), XMCD and its integral. The XMCD spectrum of Fe metal is shown for comparison (Ref. 27). (b) XMCD spectrum of the ZnO:Fe nanoparticles compared with the XMCD spectra of $\gamma\text{-Fe}_2\text{O}_3$ (Ref. 28) and Fe_3O_4 (Ref. 29).

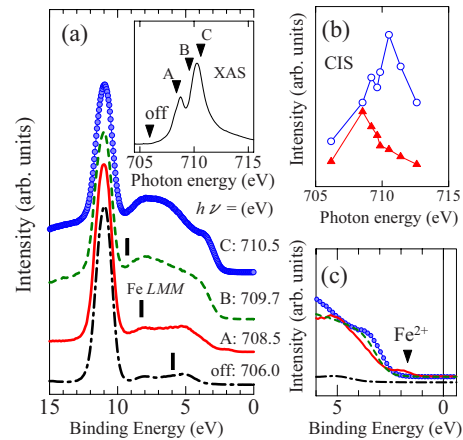


FIG. 4. (Color online) Valence-band photoemission spectra of the ZnO:Fe nanoparticles. (a) A series of photoemission spectra for photon energies in the Fe 2*p*-3*d* core-excitation region. Inset panel shows the Fe 2*p*-3*d* XAS spectrum. (b) CIS spectra at $E_B \sim 4.2$ (circle) and 2 (triangle) eV, respectively. (c) Magnified view near the valence-band maximum.

tra of the ZnO:Fe nanoparticles for opposite magnetization directions recorded using circular polarized x-rays, their difference spectrum, i.e., XMCD spectrum, and its integration. Here, the XAS spectra obtained in the magnetic field of +1 and -1 T are denoted by σ^+ and σ^- , respectively. The bottom panel shows the XMCD spectrum of Fe metal.²⁷ In the XMCD spectrum of the nanoparticles, three sharp peaks around $h\nu=708.5$, 709.7, and 710.5 eV, denoted by A, B, and C, respectively, are observed. The XMCD spectral line shape of the ZnO:Fe nanoparticles is different from that of Fe metal, indicating that the magnetism in this sample is not due to segregation of metallic Fe clusters but due to the ionic Fe atoms with localized 3*d* electrons. We note that the line shape of the XMCD spectrum recorded in point by point with reversing fields (not shown here) agreed with the one recorded in the two opposite magnetization directions reported here.

Figure 3(b) shows the Fe 2*p*-3*d* XMCD spectrum of the ZnO:Fe nanoparticles in comparison with those of $\gamma\text{-Fe}_2\text{O}_3$ nanoparticles,²⁸ where Fe^{3+} ions are both at the tetrahedral (T_d) and octahedral (O_h) sites, and Fe_3O_4 ,²⁹ where Fe^{3+} ions at the T_d and O_h sites and Fe^{2+} ions at the O_h sites coexist. The XMCD spectrum of the Fe_3O_4 , which displays the overlapping contributions from the Fe^{3+} and Fe^{2+} ions, is different from that of the ZnO:Fe nanoparticles. On the other hand, the spectral line shape of the $\gamma\text{-Fe}_2\text{O}_3$ nanoparticles, where XMCD signals are due to Fe^{3+} , is similar to that of the ZnO:Fe nanoparticles. This indicates that the magnetism of the ZnO:Fe nanoparticles originated mainly from Fe^{3+} ions and contribution from Fe^{2+} ions appears to be small. By comparison with the Fe 2*p*-3*d* XMCD spectral shape of the $\gamma\text{-Fe}_2\text{O}_3$ nanoparticles, peaks B and C for the ZnO:Fe nanoparticles are assigned to Fe^{3+} ions at the T_d and O_h sites, respectively. Although it is likely that peak A arises mainly from $\text{Fe}^{3+}(O_h)$ ions, the present Fe 2*p*-3*d* RPES result, which is described below, suggests that peak A may be attributed not only to $\text{Fe}^{3+}(O_h)$ but also to a small amount of $\text{Fe}^{2+}(T_d)$ ions.

Figure 4(a) shows the valence-band photoemission spec-

tra of the ZnO:Fe nanoparticles taken with various photon energies in the Fe $2p$ - $3d$ core-excitation region. The Fe $2p$ - $3d$ XAS spectrum in the same energy region and the CIS spectra at $E_B \sim 4.2$ (circle) and 2 (triangle) eV are shown in Figs. 4(a) and 4(b), respectively. The photoemission spectra were taken using photon energies denoted by A, B, and C in Fe $2p$ - $3d$ XAS spectrum and at off-resonance ($h\nu = 706.0$ eV). For all the spectra, no photoemission intensity was observed at E_F , indicating the localized nature of the carriers. The off-resonance spectrum of the ZnO:Fe nanoparticles is similar to that of ZnO showing a sharp peak at about $E_B \sim 11$ eV due to the Zn $3d$ states, as well as a broad feature at $E_B \sim 4$ -9 eV due to the O $2p$ band.³⁰ If the photon energy is tuned to peak A ($h\nu = 708.5$ eV), one can see a feature at $E_B \sim 2$ eV in the on-resonance spectrum [see Fig. 4(c)], indicating that the intensity of photoelectrons arising from Fe^{2+} ions (the minority-spin state of Fe^{2+} ions)³¹ is enhanced. For the spectra excited by photon energies corresponding to peaks B ($h\nu = 709.7$ eV) and C ($h\nu = 710.5$ eV), one can see a broad structure around $E_B \sim 3$ -8 eV [see Fig. 4(a)]. The spectral line shapes excited by photon energies corresponding to B and C are similar to each other, indicating that on-resonant spectral line shape strongly depends on the valency of Fe ions rather than coordination as anticipated. Features due to Fe $L_3M_{4,5}M_{4,5}$ Auger-electron emission are marked by vertical bars in Fig. 4(a). Since these features in the on-resonance spectra are observed around $E_B > \sim 8$ eV, the enhanced features around $E_B \sim 2$ -8 eV in our RPES spectra are not due to Auger emission but is due to resonance photoemission. Indeed, the line shape of the CIS spectrum (triangle) is similar to that of the calculated Fe^{2+} XAS spectrum, while the other one (circle) is to that of the Fe^{3+} [see Fig. 6(a)]. To clarify the electronic structure associated with the Fe $3d$ ion in each valence state and crystallographic site in the ZnO:Fe nanoparticles, we have performed configuration-interaction cluster-model calculations to deduce the Fe $3d$ PDOS of each component.^{32,33}

Figure 5 shows the Fe $3d$ PDOS (open circles) of the ZnO:Fe nanoparticles, which has been obtained by subtracting the off-resonance spectrum from the on-resonance ones of $\text{Fe}^{3+}(O_h)$, $\text{Fe}^{3+}(T_d)$, and $\text{Fe}^{2+}(T_d)$, respectively. Calculated spectra (solid curves) are also shown in the same figure. Electronic structure parameters used in the calculations are listed in Table I. For the Fe^{3+} (T_d and O_h sites) ions in the ZnO:Fe nanoparticles, the values of the on-site $3d$ - $3d$ Coulomb energy U_{dd} and the $3d$ - $2p$ Coulomb energy U_{dc} on the Fe ion have been taken from the literature on the photoemission study of Fe_3O_4 ,²⁹ where Fe^{3+} ions at the T_d and O_h sites and Fe^{2+} ions at the O_h sites coexist. In addition to this, based on the RPES results, we have chosen values for the charge-transfer energy Δ of the Fe^{3+} (T_d and O_h sites) ions. The electronic structure parameters (U_{dd} , U_{dc} , and Δ) of the $\text{Fe}^{2+}(T_d)$ ions were appropriately chosen to reproduce the RPES result since there is no information in the literature about the electronic structure parameters of the $\text{Fe}^{2+}(T_d)$ ions. The Δ value of the $\text{Fe}^{2+}(T_d)$ ions thus employed is large compared to those of the $\text{Fe}^{3+}(T_d)$ ions, consistent with the systematic decrease in the Δ value as the ionic charge

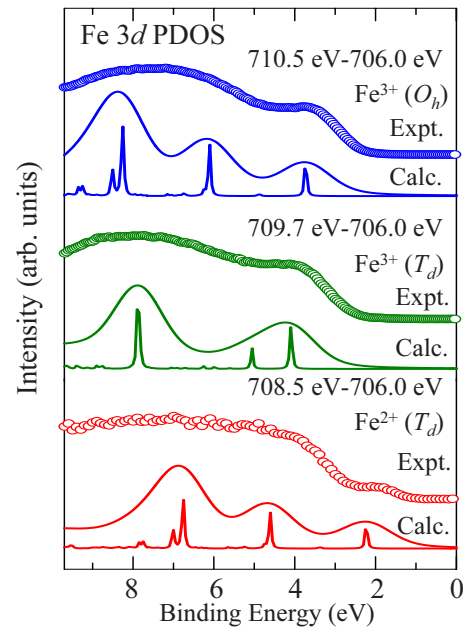


FIG. 5. (Color online) Differences between the on-resonance spectra taken with photon energies marked by A, B and C in Fig. 4(a) and off-resonance one corresponding to the PDOS of the Fe ion in each valence state and crystallographic sites. Open circles represent experimental data and thin solid curves indicate calculated spectra.

increases.³⁴ The calculated spectra have been broadened with a Gaussian having a full width at half maximum (FWHM) of 0.6 eV and with a Lorentzian having a FWHM of 0.2 eV. The spectral line shapes of the calculated results agree with those of experimental results, confirming the presence of the $\text{Fe}^{3+}(O_h)$, $\text{Fe}^{3+}(T_d)$, and $\text{Fe}^{2+}(T_d)$ ions.

Figures 6(a) and 6(b) show the Fe $2p$ - $3d$ XAS and XMCD spectra of the ZnO:Fe nanoparticles compared with the calculated spectra of the $\text{Fe}^{3+}(O_h)$, $\text{Fe}^{3+}(T_d)$, and $\text{Fe}^{2+}(T_d)$ ions. The calculations have been made using parameters listed in Table I. One observes shifts of the peaks in the XAS and XMCD spectra for the three kinds of the Fe ions, $\text{Fe}^{3+}(T_d)$, $\text{Fe}^{3+}(O_h)$, and $\text{Fe}^{2+}(T_d)$. The center of gravity of each spectrum is affected by Madelung energy, U_{dd} and U_{dc} at the Fe site, whereas the peak position may be shifted by crystal-field splitting.²⁹ Therefore, both the coordination and the valence state of the Fe ion affect the XAS and XMCD peak positions. Thus, one can clearly distinguish between the valence and crystal-field of Fe ion [$\text{Fe}^{3+}(T_d)$, $\text{Fe}^{3+}(O_h)$, and $\text{Fe}^{2+}(T_d)$]. In Fig. 6(a), the weighted sum of the calculated $\text{Fe}^{3+}(O_h)$: $\sim 65\%$, $\text{Fe}^{3+}(T_d)$: $\sim 15\%$, and $\text{Fe}^{2+}(T_d)$: $\sim 20\%$ XAS spectra shown at the bottom of panel (a) approximately reproduces the measured XAS spectrum. These ratios indicate that Fe ions are predominantly in the Fe^{3+} state with mixture of a small amount of Fe^{2+} . Since the nanoparticles are expected to have a relatively thick (~ 0.5 -1 nm) surface region of the particles and large surface area, the XAS and XMCD signals come mainly from the shell (Fe^{3+}) region of the nanoparticles. In Fig. 6(b), the weighted sum of the calculated $\text{Fe}^{3+}(O_h)$: $\sim 65\%$, $\text{Fe}^{3+}(T_d)$: $\sim 25\%$, and $\text{Fe}^{2+}(T_d)$: $\sim 10\%$ XMCD spectra shown at the bottom of panel (b) approximately reproduces the measured XMCD spectrum. However, the feature around $h\nu$

TABLE I. Electronic structure parameters for the ZnO:Fe nanoparticles used in the cluster-model calculations in units of eV. The charge-transfer energy Δ , the on-site $3d$ - $3d$ Coulomb energy U_{dd} , and the $3d$ - $2p$ Coulomb energy U_{dc} on the Fe ion, the hybridization strength between Fe $3d$ and O $2p$ $pd\sigma$, and the crystal-field $10Dq$.

	Δ	U_{dd}	U_{dc}	$pd\sigma$	$10Dq$
$\text{Fe}^{3+}(O_h)$	2.0	6.0	7.5	-3.2	0.9
$\text{Fe}^{3+}(T_d)$	3.5	6.0	7.5	-1.7	-0.7
$\text{Fe}^{2+}(T_d)$	6.5	5.5	6.9	-1.3	-0.7

~ 724 eV ($2p_{1/2}$) in the measured XMCD spectrum is weaker than the calculated one, indicating that the orbital magnetic moment due to the Fe ions in the ZnO:Fe nanoparticles is not negligible.²⁷ The sizable contribution of the orbital moment to the magnetic moment is a distinct trend of nanoparticle systems.³⁵ They have reported that the enhancement of orbital magnetism is largely determined by the contribution of surface atoms and the larger spin-orbit coupling of the electrons at surface atoms in the nanoparticle can affect the magnetic ordering in the nanoparticles.³⁵

Figure 7(a) shows the Fe $2p$ - $3d$ XMCD spectra of the ZnO:Fe nanoparticles measured at various magnetic fields. One can observe the XMCD intensity down to $H \sim 0.1$ T, as shown in Figs. 7(a) and 7(b), indicating that the ferromagnetism in this sample is originated from the ionic Fe atoms. The difference between the XMCD spectra at $H \sim 1$ and 0.5 T reflects the paramagnetic (PM) components, as shown in Fig. 7(c). From the line shape of the PM components analyzed with the cluster-model calculation, we conclude that the paramagnetism in the ZnO:Fe nanoparticles is originated from the Fe^{3+} ions (O_h : $\sim 75\%$ and T_d : $\sim 25\%$) and contributions from the Fe^{2+} ions are negligible, consistent with the proposal by Karmakar *et al.*¹⁸ According to Ref. 18, the magnetization was saturated at quite high magnetizing fields ($H \sim 12$ T) in the SQUID measurements. Also, we note that one can rule out the possibility of thermal-energy induced spontaneous magnetization reversal which may happen in an assembly of single-domain particles leading to superparamagnetic behavior.¹⁸ The ferromagnetic (FM) components obtained by subtracting the PM components from the XMCD

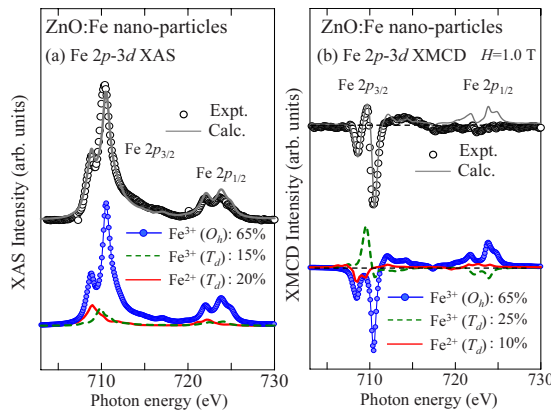


FIG. 6. (Color online) Fe $2p$ - $3d$ XAS (a) and XMCD (b) spectra of the ZnO:Fe nanoparticles compared with the calculated one using the cluster-model. Calculated spectra of the $\text{Fe}^{3+}(O_h)$, $\text{Fe}^{3+}(T_d)$ and $\text{Fe}^{2+}(T_d)$ ions at the bottom of each panel have been added to be compared with experiment. Parameters used in the calculations (Table I) were obtained from the analysis of the Fe $2p$ - $3d$ RPES spectra.

spectrum at $H \sim 0.5$ T is shown in Fig. 7(d). From the line-shape analysis, we conclude that the FM components are originated from both predominant Fe^{3+} and a small amount of Fe^{2+} ions, where the composition ratios of the $\text{Fe}^{3+}(O_h)$, $\text{Fe}^{3+}(T_d)$, and $\text{Fe}^{2+}(T_d)$ are about $\sim 60\%$, $\sim 25\%$, and $\sim 15\%$, respectively. In Fig. 7(d), peaks due to the Fe^{3+} ions at the T_d and O_h sites occur in the opposite directions. This clearly implies the presence of $\text{Fe}^{3+}(T_d)$ - $\text{Fe}^{3+}(O_h)$ antiferromagnetic coupling. Therefore, it is possible that this sample exhibits “weak ferrimagnetism” due to the Fe^{3+} ions occupying two sets of nonequivalent positions (T_d and O_h sites) in unequal numbers and in antiparallel configurations so that there is a net moment.³⁶ That is, the ferromagnetism is mainly due to the difference in the electron numbers between up and down spins at $T_d(O_h)$ and $O_h(T_d)$ sites. In addition to this, Fe^{2+} - Fe^{2+} , Fe^{3+} - Fe^{3+} exchange interactions and Fe^{3+} - Fe^{2+} double exchange interaction are considered to exist.

From the experimental and cluster-model calculation results, we have estimated the relative abundance of the magnetically compensated (MC), FM, and PM components of the Fe ions [$\text{Fe}^{3+}(O_h)$, $\text{Fe}^{3+}(T_d)$, and $\text{Fe}^{2+}(T_d)$], as shown in Fig. 8. The MC components are considered to be originated

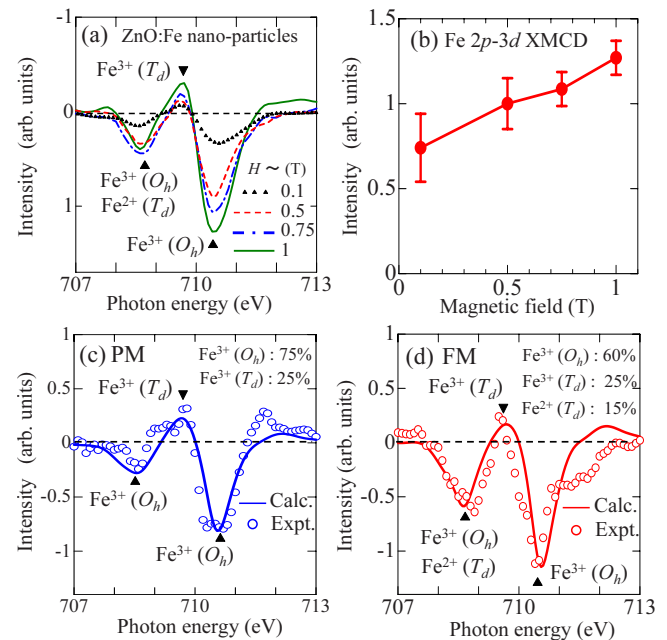


FIG. 7. (Color online) Fe $2p$ - $3d$ XMCD spectra of the ZnO:Fe nanoparticles. (a) Fe $2p$ - $3d$ XMCD spectra of the ZnO:Fe nanoparticles measured at various magnetic fields. (b) Fe $2p$ - $3d$ XMCD related magnetic moment as a function of magnetic field, obtained using the XMCD sum rule. PM (c) and FM (d) components obtained from the XMCD spectra at 1 and 0.5 T. Open circles represent experimental data and thin solid curves indicate calculated spectra.

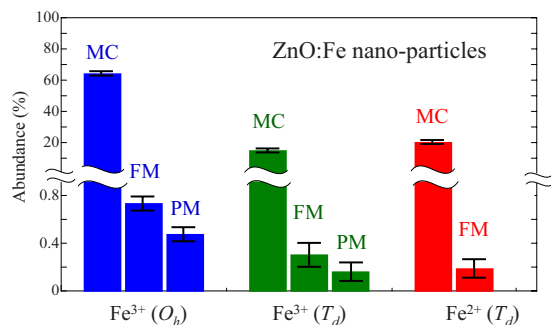


FIG. 8. (Color online) Relative abundance of the MC, FM, and PM components of the Fe ions [$\text{Fe}^{3+}(\text{O}_h)$, $\text{Fe}^{3+}(\text{T}_d)$, and $\text{Fe}^{2+}(\text{T}_d)$] in the ZnO:Fe nanoparticles.

from strongly antiferromagnetically coupled Fe ions and are dominant in this sample. The PM components are due to the uncoupled Fe^{3+} (T_d and O_h sites) ions and contributions from the Fe^{2+} ions are negligible. On the other hand, the FM components are originated mainly from Fe^{3+} (T_d and O_h sites) as well as from a small amount of $\text{Fe}^{2+}(\text{T}_d)$ ions. Now, we discuss the origin of the $\text{Fe}^{3+}(\text{T}_d)$ – $\text{Fe}^{3+}(\text{O}_h)$ antiferromagnetic coupling, which plays a leading role in the ferromagnetism of this sample. One possibility is secondary phases such as $\gamma\text{-Fe}_2\text{O}_3$, because the room temperature weak ferromagnetism of $\gamma\text{-Fe}_2\text{O}_3$ is due to $\text{Fe}^{3+}(\text{T}_d)$ – $\text{Fe}^{3+}(\text{O}_h)$ antiferromagnetic coupling.³⁷ However, from the line-shape analysis of the EPR spectra,¹⁸ the probability of large amounts of secondary phase such as Fe_2O_3 is expected to be very small. In addition, recent experimental study³⁸ has shown that for a doping percentage of up to 10%, the ferrite formation probability is unlikely in this system. The other possibility is surface-vacancy-induced ferromagnetism.^{18,39} We speculate that the surface Zn vacancies and excess oxygen may create the $\text{Fe}^{3+}(\text{T}_d)$ and $\text{Fe}^{3+}(\text{O}_h)$ ions, respectively, and $\text{Fe}^{3+}(\text{T}_d)$ – $\text{Fe}^{3+}(\text{O}_h)$ antiferromagnetic coupling occurs. If Zn vacancies, which dope the system with holes, are present near $\text{Fe}^{2+}(\text{T}_d)$ ions substituting Zn sites, the $\text{Fe}^{2+}(\text{T}_d)$ ions will be converted to $\text{Fe}^{3+}(\text{T}_d)$.^{18,39} This will occur mostly in the surface region of the nanoparticles, where the probability of the creation of vacancies is higher.¹⁸ Based on the earlier theoretical study⁴⁰ and XAS measurements⁴¹ of nanoparticles, we suggest that the presence of the $\text{Fe}^{3+}(\text{O}_h)$ ions is due to excess oxygen at the surface of the nanoparticles. According to the literature about the molecular dynamics simulations of Fe_2O_3 nanoparticles,⁴⁰ to achieve local charge neutrality, it is expected that oxygen atoms have a tendency to concentrate on the surface of the ZnO:Fe nanoparticles. If there are excess oxygen atoms, the Fe ions in the surface region of the ZnO:Fe nanoparticles would be coordinated to a larger number of oxygen atoms as if they were at the O_h sites. Indeed, Chen *et al.*⁴¹ have reported that $\text{Fe}(\text{T}_d)$ ions in the surface region of Fe_3O_4 nanoparticles have a tendency to be converted to $\text{Fe}(\text{O}_h)$. Note that the presence of $\text{Fe}(\text{O}_h)$ ions due to interstitial impurities has been excluded by EPR, XRD, and Mössbauer measurements on the same sample.¹⁸

IV. SUMMARY

We have performed XPS, RPES, XAS, and XMCD measurements on the ferromagnetic ZnO:Fe nanoparticles. The

XPS and RPES results suggest that the Fe ions are in mixed-valence (Fe^{2+} and Fe^{3+}) states and the Fe^{3+} ions are dominant in the surface region of the nanoparticles. XMCD signals due to ferromagnetism and paramagnetism were observed at the Fe 2*p* absorption edge. Based on the line-shape analysis of the FM components using the cluster-model calculation, it is found that the FM components mainly originated from both predominant Fe^{3+} (T_d and O_h sites) and a small amount of $\text{Fe}^{2+}(\text{T}_d)$ ions, and it is likely that the room temperature ferromagnetism in the ZnO:Fe nanoparticles primarily originated from the $\text{Fe}^{3+}(\text{T}_d)$ – $\text{Fe}^{3+}(\text{O}_h)$ antiferromagnetic coupling. From the line shape of the PM components analyzed with the cluster-model calculation, we find that the PM components are due to the Fe^{3+} ions (T_d and O_h sites) and contributions from the Fe^{2+} ions are negligible. The MC components are due to the strongly antiferromagnetic coupled Fe ions and are dominant in this sample. Considering that the Fe^{3+} ions are dominant in the surface region of the nanoparticles probed by Fe 3*p*–3*d* RPES and ferromagnetism in the ZnO:Fe nanoparticles is primarily originated from the $\text{Fe}^{3+}(\text{T}_d)$ – $\text{Fe}^{3+}(\text{O}_h)$ antiferromagnetic coupling, it is important to consider the surface effects of the nanoparticles for understanding of the ferromagnetism in the ZnO:Fe nanoparticles.

ACKNOWLEDGMENTS

We thank T. Koide and D. Asakura for useful discussion and comments. We thank T. Okuda and A. Harasawa for their valuable technical support for the experiment at PF. The experiment at SPring-8 was performed under the approval of the Japan Synchrotron Radiation Research Institute (JASRI) (Grant No. 2007B3825). The experiment at PF was approved by the Photon Factory Program Advisory Committee (Grant No. 2006G002). This work was supported by a Grant-in-Aid for Scientific Research in Priority Area “Creation and Control of Spin Current” (Grant No. 19048012) from MEXT, Japan and a Global COE Program “the Physical Sciences Frontier,” from MEXT, Japan and an Indo-Japan Joint Research Project “Novel Magnetic Oxide Nano-Materials Investigated by Spectroscopy and *ab-initio* Theories” from JSPS, Japan.

¹J. K. Furdyna, *J. Appl. Phys.* **64**, R29 (1988).

²H. Ohno, *Science* **281**, 951 (1998).

³T. Dietl, H. Ohno, F. Matsukura, J. Cibert, and D. Ferrand, *Science* **287**, 1019 (2000).

⁴K. Sato and H. Katayama-Yoshida, *Jpn. J. Appl. Phys., Part 2* **40**, L334 (2001).

⁵A. C. Tuan, J. D. Bryan, A. B. Pakhomov, V. Shutthanandan, S. Thevuthasan, D. E. McCready, D. Gaspar, M. H. Engelhard, J. W. Rogers, Jr., K. Krishnan, D. R. Gamelin, and S. A. Chambers, *Phys. Rev. B* **70**, 054424 (2004).

⁶K. Ueda, H. Tabata, and T. Kawai, *Appl. Phys. Lett.* **79**, 988 (2001).

⁷P. Sharma, A. Gupta, K. V. Rao, F. J. Owens, R. Sharma, R. Ahuja, J. M. Osorio, G. B. Johansson, and G. A. Gehring, *Nature Mater.* **2**, 673 (2003).

⁸D. A. Schwartz and D. R. Gamelin, *Adv. Mater.* **16**, 2115 (2004).

⁹P. V. Radovanovic and D. R. Gamelin, *Phys. Rev. Lett.* **91**, 157202 (2003).

¹⁰T. Meron and G. Markovich, *J. Phys. Chem. B* **109**, 20232 (2005).

¹¹S. K. Mandal, A. Das, T. K. Nath, D. Karmakar, and B. Satpati, *J. Appl. Phys.* **100**, 104315 (2006).

¹²S. K. Mandal, T. K. Nath, A. Das, and R. K. Kremer, *Appl. Phys. Lett.* **89**, 162502 (2006).

¹³C. Kittel, *Phys. Rev.* **70**, 965 (1946).

- ¹⁴E. M. Chudnovsky and L. Gunther, *Phys. Rev. Lett.* **60**, 661 (1988).
- ¹⁵M. A. Garcia, J. M. Merino, and E. Fernandez, *Nano Lett.* **7**, 1489 (2007).
- ¹⁶C. Q. Sun, *Prog. Solid State Chem.* **35**, 1 (2007).
- ¹⁷R. H. Kodama, A. E. Berkowitz, Jr., E. J. McNiff, and S. Foner, *Phys. Rev. Lett.* **77**, 394 (1996).
- ¹⁸D. Karmakar, S. K. Mandal, R. M. Kadam, P. L. Paulose, A. K. Rajarajan, T. K. Nath, A. K. Das, I. Dasgupta, and G. P. Das, *Phys. Rev. B* **75**, 144404 (2007).
- ¹⁹P. Gopal and N. A. Spaldin, *Phys. Rev. B* **74**, 094418 (2006).
- ²⁰J. M. D. Coey and S. A. Chambers, *MRS Bull.* **33**, 1053 (2008).
- ²¹L. C. Davis, *J. Appl. Phys.* **59**, R25 (1986).
- ²²I. Lindau and W. E. Spicer, *J. Electron Spectrosc. Relat. Phenom.* **3**, 409 (1974).
- ²³P. Graat and M. A. J. Somers, *Surf. Interface Anal.* **26**, 773 (1998).
- ²⁴T. Fujii, F. M. F. de Groot, G. A. Sawatzky, F. C. Voogt, T. Hibma, and K. Okada, *Phys. Rev. B* **59**, 3195 (1999).
- ²⁵R. J. Lad and V. E. Henrich, *Phys. Rev. B* **39**, 13478 (1989).
- ²⁶A. Fujimori, M. Saeki, N. Kimizuka, M. Taniguchi, and S. Suga, *Phys. Rev. B* **34**, 7318 (1986).
- ²⁷C. T. Chen, Y. U. Idzerda, H.-J. Lin, N. V. Smith, G. Meigs, E. Chaban, G. H. Ho, E. Pellegrin, and F. Sette, *Phys. Rev. Lett.* **75**, 152 (1995).
- ²⁸S. B. Profeta, M. A. Arrio, E. Tronc, I. Letard, C. C. D. Moulin, and P. Sainctavit, *Phys. Scr., T* **115**, 626 (2005).
- ²⁹J. Chen, D. J. Huang, A. Tanaka, C. F. Chang, S. C. Chung, W. B. Wu, and C. T. Chen, *Phys. Rev. B* **69**, 085107 (2004).
- ³⁰M. Gabas, S. Gota, J. R. R. Barrado, M. Sanchez, and N. T. Barrett, *Appl. Phys. Lett.* **86**, 042104 (2005).
- ³¹J. Takaobushi, M. Ishikawa, S. Ueda, E. Ikenaga, J.-J. Kim, M. Kobata, Y. Takeda, Y. Saitoh, M. Yabashi, Y. Nishino, D. Miwa, K. Tamasaku, T. Ishikawa, I. Satoh, H. Tanaka, K. Kobayashi, and T. Kawai, *Phys. Rev. B* **76**, 205108 (2007).
- ³²A. Tanaka and T. Jo, *J. Phys. Soc. Jpn.* **63**, 2788 (1994).
- ³³A. Tanaka and T. Jo, *J. Phys. Soc. Jpn.* **61**, 2669 (1992).
- ³⁴A. E. Bocquet, T. Mizokawa, T. Saitoh, H. Namatame, and A. Fujimori, *Phys. Rev. B* **46**, 3771 (1992).
- ³⁵C. F. J. Flipse, C. B. Rouwelaar, and F. M. F. de Groot, *Eur. Phys. J. D* **9**, 479 (1999).
- ³⁶M. A. Gilleo, *Phys. Rev.* **109**, 777 (1958).
- ³⁷X. Bo, G. Li, X. Qiu, Y. Xue, and L. Li, *J. Solid State Chem.* **180**, 1038 (2007).
- ³⁸D. Karmakar, T. V. C. Rao, J. V. Yakhmi, A. Yaresko, V. N. Antonov, R. M. Kadam, S. Mandal, R. Adhikari, A. K. Das, T. K. Nath, N. Chatterjee, I. Dasgupta, and G. P. Das (unpublished).
- ³⁹N. Ganguli, I. Dasgupta, and B. Sanyal, *Appl. Phys. Lett.* **94**, 192503 (2009).
- ⁴⁰B. T. H. L. Khanh, V. V. Hoang, and H. Zung, *Eur. Phys. J. D* **49**, 325 (2008).
- ⁴¹L. X. Chen, T. Liu, M. C. Thurnauer, R. Csencsits, and T. Rajh, *J. Phys. Chem. B* **106**, 8539 (2002).